Small angle X-ray scattering beamline at SSRF (Postprint)

Authors: TIAN Feng, LI Xiu-Hong, WANG Yu-Zhu, YANG Chun-Ming, ZHOU Ping, LIN Jin-You, Jianrong Zeng, HONG Chun-Xia, HUA Wen-Qiang, LI Xiao-Yun, MIAO Xia-Ran, BIAN Feng-Gang, WANG Jie

Date: 2023-06-18T00:00:00+00:00

Abstract

Beamline BL16B1 at Shanghai Synchrotron Radiation Facility (SSRF) is dedicated to small angle X-ray scattering (SAXS) study. It aims at probing microstructure and dynamic processes of polymers, nanomaterials, mesoporous materials, colloids, liquid crystals, metal materials, etc. At present, SAXS, wide angle X-ray scattering (WAXS), simultaneous SAXS/WAXS, grazing incident SAXS, and anomalous SAXS techniques are available. The sample-to-detector distance is adjustable from 0.2 m to 5 m. For conventional SAXS, the practicable q-range is from 0.03–3.6 nm-1 at incident X-ray of 10 keV. A continuous q-region of 0.06–33 nm-1 can be achieved in simultaneous SAXS/WAXS mode. Time-resolved SAXS measurements in sub-second level can be performed. Detailed descriptions about status, performance and application of the SAXS beamline are given in this paper.

Full Text

Preamble

Small Angle X-ray Scattering Beamline at SSRF

Tian Feng, Li Xiu-Hong, Wang Yu-Zhu, Yang Chun-Ming, Zhou Ping, Lin Jin-You, Zeng Jian-Rong, Hong Chun-Xia, Hua Wen-Qiang, Li Xiao-Yun, Miao Xia-Ran, Bian Feng-Gang,† and Wang Jie

Shanghai Institute of Applied Physics, Chinese Academy of Sciences, Shanghai 201204, China

(Received September 30, 2014; accepted in revised form April 9, 2015; published online June 20, 2015)

Beamline BL16B1 at the Shanghai Synchrotron Radiation Facility (SSRF) is dedicated to studying the microstructure and dynamic processes of polymers, nanomaterials, mesoporous materials, colloids, liquid crystals, metal materials, and other systems. Currently, SAXS, wide-angle X-ray scattering (WAXS), simultaneous SAXS/WAXS, grazing-incidence SAXS, and anomalous SAXS techniques are available for users to conduct diverse experiments. The sample-to-detector distance is adjustable from 0.2 m to 5 m, providing a practical q-range of 0.03–3.6 nm^{-1} at an incident X-ray energy of 10 keV for conventional SAXS, while a continuous q-region of 0.06–33 nm^{-1} can be achieved in simultaneous SAXS/WAXS mode. Time-resolved SAXS measurements at the sub-second level were enabled by a beamline upgrade in 2013. This paper provides a detailed description of the status, performance, and applications of the SAXS beamline.

Keywords: Small angle X-ray scattering (SAXS), Wide angle X-ray scattering, Grazing incident SAXS, Anomalous SAXS

DOI: 10.13538/j.1001-8042/nst.26.030101

Introduction

As a third-generation synchrotron radiation light source, the Shanghai Synchrotron Radiation Facility (SSRF) [1] now operates in top-up injection mode with a constant electron beam current of 240 mA. The small-angle X-ray scattering (SAXS) beamline (BL16B1) is one of the seven Phase-I beamlines at SSRF, designed for measurements of small-angle X-ray scattering (SAXS), wide-angle X-ray scattering (WAXS), anomalous small-angle X-ray scattering (ASAXS), and grazing-incidence small-angle X-ray scattering (GISAXS) on appropriate samples. Constructed and opened to users in 2009 and upgraded in 2013, the beamline enables time-resolved studies of structural transitions at the sub-second level. Most user experiments performed on this beamline involve kinetics, dynamics, and rheology of materials with nanoscale structures, such as polymers, nanomaterials, mesoporous materials, colloids, liquid crystals, and metal materials. This paper presents a detailed description of the SAXS beamline and experimental station.

II. Beamline Configuration and Technique Specifications

The photon source from the SSRF bending magnet delivers X-rays in the 5–20 keV range. The optics system can accept a beam with 1.2×0.12 $mrad^2$ divergence. The beamline optics consist of a Si(111) flat double-crystal monochromator (DCM) and a double-focusing toroidal mirror. The optical layout of the beamline is shown in Fig. 1 [FIGURE:1]. Generally, the beamline operates at 10 keV (0.124 nm) for user experiments.

The specifications of the SAXS beamline are as follows: energy range 5–20 keV; energy resolution 4.0×10^{-4} @ 10 keV; flux 3×10^{11} phs/s @ 10 keV and 240

mA; and focus size 0.4 mm (H) × 0.5 mm (V). The measured spot size and rocking curve results for BL16B1 are shown in Fig. 2 [FIGURE:2].

The BL16B1 endstation is shown in Fig. 3 [FIGURE:3]. The detectors include a Mar165 CCD for SAXS and an INEL CPS120 (a one-dimensional arc gas detector) for WAXS. The beam intensity monitor before the sample is an N_2 gas ionization chamber, while the monitor after sample absorption is a photodiode in the beam stop. Two scatter-less slits (Xenocs) are used to suppress parasitic scattering. The sample holder is mounted on an optical table, and the sample-to-SAXS detector distance can be adjusted up to 5 m. Scattering from a sample transmits through vacuum, passing a Kapton window to reach the detector. Sample stages are available for SAXS, GISAXS, or WAXS (2D). The q ranges are 0.03–3.6 nm^{-1} for SAXS measurement and 4.5–33 nm^{-1} for WAXS measurement at 10 keV. A continuous q range of 0.06–33 nm^{-1} can be obtained in simultaneous SAXS/WAXS mode. Two conventional sample-to-detector distances of 2 m and 5 m are provided to users, offering q ranges of 0.08–3.6 nm^{-1} at 2 m and 0.03–1.4 nm^{-1} at 5 m.

The beamline control system is based on an EPICS platform in a Linux operating system, which facilitates communication among devices. The CPS 120 detector currently operates on a LabVIEW platform in a Windows environment but will be integrated into EPICS in the future. In addition to the provided sample environments, users have the option to install their own specialized sample devices [2–5]. Technical boundary conditions, user-friendliness, and reliability have been considered important design criteria.

III. Methodology

The beamline supports several techniques including SAXS, WAXS, simultaneous SAXS/WAXS, GISAXS, and ASAXS.

A. SAXS Technique

SAXS in transmission mode can be used to study materials such as polymers, nanomaterials, metals, and biomaterials [6–10]. Most SAXS experiments performed are in-situ studies of microstructural evolution in different samples, such as in-situ stretching of polymers and fibers at various temperatures. A typical study [11] investigated the long-time evolution of extension-induced crystallization in polyethylene oxide (PEO) by combining rheological measurements with in-situ SAXS to understand dynamic changes in the spatial arrangement of nuclei in terms of chain stretching and orientation. The structural evolution in the small-strain region is shown in Fig. 4 [FIGURE:4].

B. Simultaneous SAXS/WAXS Measurement

Figure 5 FIGURE:5 shows the instrumentation schematic for simultaneous SAXS/WAXS measurement. To obtain a continuous scattering vector q across

the SAXS and WAXS collectable regions, the simultaneous SAXS/WAXS technique was developed, with the determinable SAXS range being q = 0.06–3.50 nm^{-1} and the WAXS range being q = 2.50–34.8 nm^{-1}. Consequently, a continuous q range of 0.06–33 nm^{-1} can be achieved (Fig. 5(b)). Simultaneous SAXS/WAXS is important for studying fiber stretching, liquid crystals, and self-assembly systems [12, 13].

The hardware configuration is shown schematically in Fig. 6 [FIGURE:6]. The Mar165 CCD serves as the SAXS detector, while the 1D arc PSD (CPS 120) is the WAXS detector. The SAXS detector provides a trigger signal to control other equipment synchronously. The shutter, WAXS detector, and SAXS detector can operate synchronously through a pulse generator. Experimental results of simultaneous SAXS/WAXS for silver behenate performed on BL16B1 are shown in Fig. 5(b). The SAXS and WAXS data are combined by scaling the SAXS data with a factor to equalize their integrated area in the overlap region.

C. Grazing Incidence SAXS

GISAXS is a powerful tool for studying film surface and interface structures [14-17]. A Kohzu tilt stage is used as the GISAXS sample stage (Fig. 7 [FIGURE:7]). The X-ray incidence angle can be adjusted by the sample stage with an accuracy of 0.001°. In principle, sample sizes should be larger than 0.5 cm (width) × 1 cm (length).

GISAXS experiments [18-21] performed on BL16B1 include the discovery of a novel orientation of mesochannels in mesostructured thin films, with results published in [22]. As shown in Fig. 8(a)

, uniaxially oriented mesoporous titania films in any alignment direction were prepared by manipulating the magnitude and incidence angle of a shear force from hot air flow. According to the TEM and GISAXS results in Figs. 8(b)-8(e), the mesochannel orientation can be well controlled into parallel, vertical, or oblique alignments at any angle with respect to the plane by simply regulating the flow rate and incident angle of the air flow.

A one-dimensional profile along the vertical and horizontal directions can be extracted from a two-dimensional GISAXS pattern using "Pre-GISAXS" (Fig. 9 [FIGURE:9]) [23].

D. Anomalous SAXS

ASAXS measurements can be conducted utilizing the beamline's energy tunability. ASAXS studies have been performed on aluminum alloys (7150 and 7085 Al alloys). SAXS patterns of 7150 Al alloy were obtained at various energies below the Zn K-edge. The scattering intensity increased significantly with decreasing energy. Due to absorption, the alloy sample thickness should be less than 150 μm.

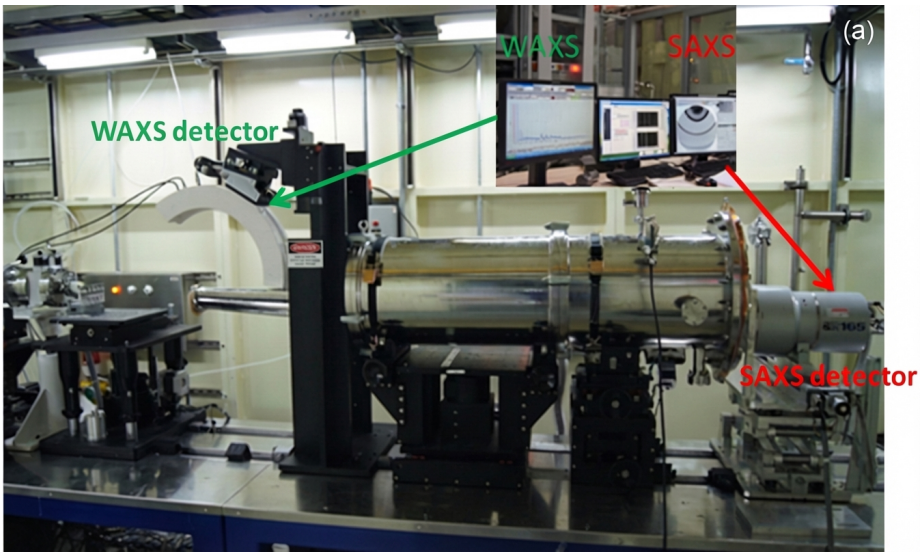

Figure 1: Figure 8

E. SAXS Study of Protein Solution

To reduce radiation damage, we have developed a peristaltic device with temperature control for solution SAXS measurements (Fig. 10(a) [FIGURE:10]) [24]. Figures 10(b)-10(d) show scattering data for lysozyme collected at BL16B1 using this device, demonstrating its ability to reduce radiation damage for biomacromolecular solution samples.

F. Supporting Conditions and Data Processing

The BL16B1 beamline at SSRF provides comprehensive support for users to conduct experimental research. Samples can be prepared in support laboratories equipped with an ultra-pure water system, magnetic stirrer, electronic balance, ultrasonic apparatus, centrifuge, electric oven, vacuum drying apparatus, polarizing microscope, and AFM. Available in-situ devices include a Linkam THMS600 heating stage (−196 °C to 600 °C), Linkam CSS450 shearing system (ambient to 450 °C), Linkam TS1500 heating stage (ambient to 1500 °C), an in-situ fiber stretching device (maximum tension: 1000 N, ambient to 500 °C), and a helium-atmosphere sample chamber to protect samples from oxidation.

Several widely-used data processing packages have been developed, including Irena, Nika, X-polar, and FIT2D. Special data processing services such as remote data access and data archiving [25] are also available upon request.

IV. Conclusion

The SAXS beamline at SSRF provides powerful capabilities for studying the microstructure of polymers, fibers, and nanostructured/mesoporous materials. Available techniques include SAXS, WAXS, ASAXS, GISAXS, and time-resolved simultaneous SAXS/WAXS for investigating structural transitions in the sub-second time regime and partially ordered systems with real-space dimensions ranging from 1 nm to 240 nm. Additional techniques will be developed at BL16B1, such as USAXS based on a Bonse-Hart camera system and micro-focus SAXS. More common in-situ devices will be developed to facilitate users, and a complete SAXS data analysis platform will be established for data pretreatment and SAXS/WAXS data analysis.

References

[1] Xu H J and Zhao Z T. Current status and progresses of SSRF project. Nucl Sci Tech, 2008, 19: 1-6. DOI: 10.1016/S1001-8042(08)60013-5

[2] Liu G M, Zheng L C, Zhang X Q, et al. Critical stress for crystal transition in poly(butylene succinate)-based crystalline–amorphous multiblock copolymers. Macromolecules, 2014, 47: 7533–7539. DOI: 10.1021/ma501832z

[3] Li F G, Zhang J, Dai Y B, et al. Study of the influence of TiB_2 particles on the melt structure of the hypoeutectic Al–Cu alloy by small angle X-ray scattering. Mater Chem Phys, 2014, 143: 471–475. DOI: 10.1016/j.matchemphys.2013.10.027

[4] Wei Z Z, Lin J Y, Tian F, et al. Synchronous stimuli of biodegradable poly(butylene succinate-co-terephthalate) copolymer via uniaxial stretching at varying temperatures. J Polym Sci Pol Phys, 2014, 9: 640–649. DOI: 10.1002/polb.23681

[5] Huang Y F, Xu J Z, Xu J Y, et al. Self-reinforced polyethylene blend for artificial joint application. J Mater Chem B, 2014, 2: 971–980. DOI: 10.1039/C3TB21231A

[6] Pan H, Zhang Y P, Shao H L, et al. Nanoconfined crystallites toughen artificial silk. J Mater Chem B, 2014, 2: 1408–1414. DOI: 10.1039/C3TB21148G

[7] Shen J L, Xu L F, Wang C P, et al. Dynamic and quantitative control of the DNA-mediated growth of gold plasmonic nanostructures. Angew Chem Int Edit, 2014, 32: 8338–8342. DOI: 10.1002/anie.201402937

[8] Liu D M, Xiong B Q, Bian F G, et al. In situ studies of microstructure evolution and properties of an Al–7.5Zn–1.7Mg–1.4Cu–0.12Zr alloy during retrogression and reaging. Mater Design, 2014, 56: 1020–1024. DOI: 10.1016/j.matdes.2013.12.006

[9] Su H Y, Liu Y H, Wang D, et al. Amphiphilic starlike dextran wrapped superparamagnetic iron oxide nanoparticle clusters as effective magnetic

resonance imaging probes. Biomaterials, 2013, 34: 1193–1203. DOI: 10.1016/j.biomaterials.2012.10.056

[10] Liu F, Prehm M, Zeng X B, et al. Skeletal cubic, lamellar, and ribbon phases of bundled thermotropic bolapolyphiles. J Am Chem Soc, 2014, 136: 6846–6849. DOI: 10.1021/ja502410e

[11] Tian N, Liu D, Li X Y, et al. Relaxation propelled long period change in the extension induced crystallization of polyethylene oxide. Soft Matter, 2013, 9: 10759–10767. DOI: 10.1039/C3SM52152D

[12] Leonard M J and Strey H H. Phase diagrams of stoichiometric polyelectrolyte–surfactant complexes. Macromolecules, 2003, 36: 9549–9558. DOI: 10.1021/ma034352c

[13] Shi Z H, Cheng D Z, Lu H J, et al. Self-assembled hierarchical structure evolution of azobenzene-containing linear-dendritic liquid crystalline block copolymers. Soft Matter, 2012, 8: 6174–6184. DOI: 10.1039/C2SM07249A

[14] Zhang J Q, Posselt D, Smilgies DM, et al. Lamellar diblock copolymer thin films during solvent vapor annealing studied by GISAXS: different behavior of parallel and perpendicular lamellae. 2014, 47: 5711–5718. DOI: 10.1021/ma500633b

[15] Huang Y C, Tsao C S, Chuang C M, et al. Small- and wide-angle X-ray scattering characterization of bulk heterojunction polymer solar cells with different fullerene derivatives. J Phys Chem C, 2012, 116: 10238–10244. DOI: 10.1021/jp210140j

[16] Ahn B, Hirai T, Jin S, et al. Hierarchical structure in nanoscale thin films of a poly(styrene-b-methacrylate grafted with POSS) (PS214-b-PMAPOSS27). Macromolecules, 2010, 43: 10568–10581. DOI: 10.1021/ma101276d

[17] Liang Y Y, Feng D Q, Guo J C, et al. Regioregular oligomer and polymer containing thieno[3,4-b]thiophene moiety for efficient organic solar cells. Macromolecules, 2009, 42: 1091–1098. DOI: 10.1021/ma8023969

[18] Dou J H, Zheng Y Q, Lei T, et al. Systematic investigation of side-chain branching position effect on electron carrier mobility in conjugated polymers. Adv Funct Mater, 2014, 40: 6270–6278. DOI: 10.1002/adfm.201401822

[19] Shan F, Lu X M, Guan J F, et al. Airflow-field-induced sandwich-type membrane of block copolymer for selective ion separation. Macromol Rapid Comm, 2014, 35: 735–740. DOI: 10.1002/marc.201300880

[20] Sun J H, Zhang Q H, Ding R M, et al. Contamination-resistant silica antireflective coating with closed ordered mesopores. Phys Chem Chem Phys, 2014, 16: 16684–16693. DOI: 10.1039/c4cp01032a

[21] He Q Y, Dai H, Tan X P, et al. Synthesis and characterization of room temperature columnar mesogens of cyclotriphosphazene with Schiff base units. J Mater Chem C, 2013, 1: 7148–7154. DOI: 10.1039/C3TC31371A

[22] Shan F, Lu X M, Zhang Q, et al. A facile approach for controlling the orientation of one-dimensional mesochannels in mesoporous titania films. J Am Chem Soc, 2012, 134: 20238–20241. DOI: 10.1021/ja309168f

[23] Zhao N, Bian F G, Wang Y Z, et al. Calibrating scattering angle in wide angle X-ray scattering experiment. Sci China Ser G-Phys Mech Astron, 2015, 45: 017001. (in Chinese) DOI: 10.1360/SSPMA2014-00106

[24] The resource for macromolecular SAXS. http://www.bioisis.net/tutorial

[25] HU Z, MI Q, ZHENG L, et al. EPICS data archiver at SSRF beamlines. Nucl Sci Tech, 2014, 25: 020103. DOI: 10.13538/j.1001-8042/nst.25.020103

Figures

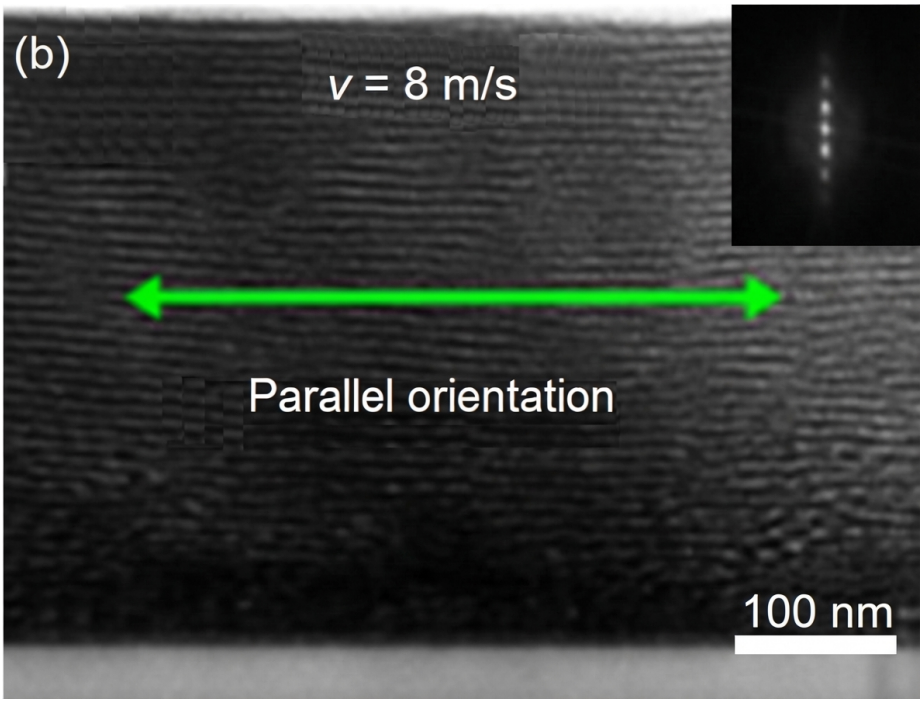

Figure 2: Figure 13

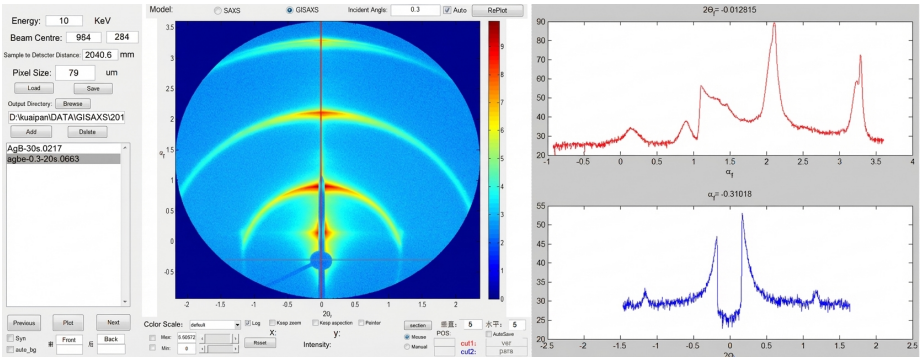

Figure 3: Figure 17